Tiny Grains Give Huge Gains: Nanocrystal-Based Signal Amplification for Biomolecule Detection

Sheng Tong, Binbin Ren, Zhilan Zheng, Han Shen, and Gang Bao*

Department of Biomedical Engineering, Georgia Institute of Technology and Emory University, Atlanta, Georgia 30332, United States

ABSTRACT Nanocrystals, despite their tiny sizes, contain thousands to millions of atoms. Here we show that the large number of atoms packed in each metallic nanocrystal can provide a huge gain in signal amplification for biomolecule detection. We have devised a highly sensitive, linear amplification scheme by integrating the dissolution of bound nanocrystals and metal-induced stoichiometric chromogenesis, and demonstrated that signal amplification is fully defined by the size and atom density of nanocrystals, which can be optimized through well-controlled nanocrystal synthesis. Further, the rich library of chromogenic reactions allows implementation of this scheme in various assay formats, as demonstrated by the iron oxide nanoparticle linked immunosorbent assay (ILISA) and blotting assay developed in this study. Our results indicate that, owing to the inherent simplicity, high sensitivity and repeatability, the nanocrystal based amplification scheme can significantly improve biomolecule quantification in both laboratory research and clinical diagnostics. This novel method adds a new dimension to current nanoparticle-based bioassays.

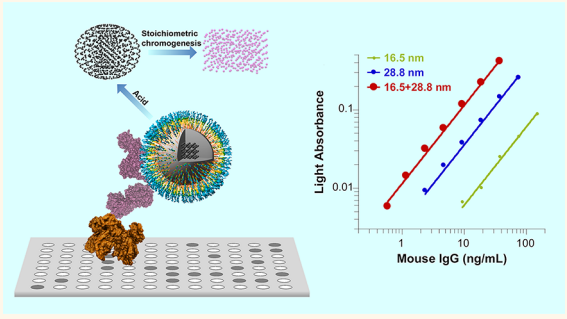

KEYWORDS: nanocrystal · detection · signal amplification

In the past decade, biomolecule detection has become increasingly important in biological studies and clinical applications. In particular, the expressions of lipids, proteins and nucleotides are widely adopted as criteria in disease diagnosis and management, which require sensitive and quantitative determination of the level of these molecular markers.[1,2] Traditional detection assays relying on small-molecule reporters such as radioisotopes and fluorophores have found little use in these applications because of poor stability, low sensitivity and difficult sample processing. The need for simple and reliable detection methods has led to the development of various inorganic nanoparticle-based probes. With remarkable magnetic, optical or plasmonic properties, these nanoparticles have greatly expanded the scope of specific bioassays.[3−5] For instances, quantum dots and gold nanoparticles can drastically increase the sensitivity of immunofluorescence staining, microarrays and microfluidics.[6−8] Magnetite and maghemite nanoparticles are being utilized for on-site detection of proteins, nucleotides and bacteria,[9] in addition to enriching target molecules in detection assays.[6,10]

Due to the low intrinsic signal of biomolecules, most existing detection techniques are based on a tagging strategy that links the target molecule to reporters. The number of target molecules is then converted to a specific measure, be it fluorescence signal, radioactivity, or electric current. The ratio between the bound reporters and the target molecules determines the fold of amplification and hence the detection sensitivity of the assay. According to amplification schemes, existing detection techniques can be divided into two categories: direct amplification and enzymatic amplification. In direct amplification, the reporters are conjugated or adsorbed to the surface of detection probes (Scheme 1A). Owing to steric hindrance, the fold of amplification rarely

* Address correspondence to gang.bao@bme.gatech.edu.

Received for review February 13, 2013 and accepted May 9, 2013.

Published online May 09, 2013
10.1021/nn400733t

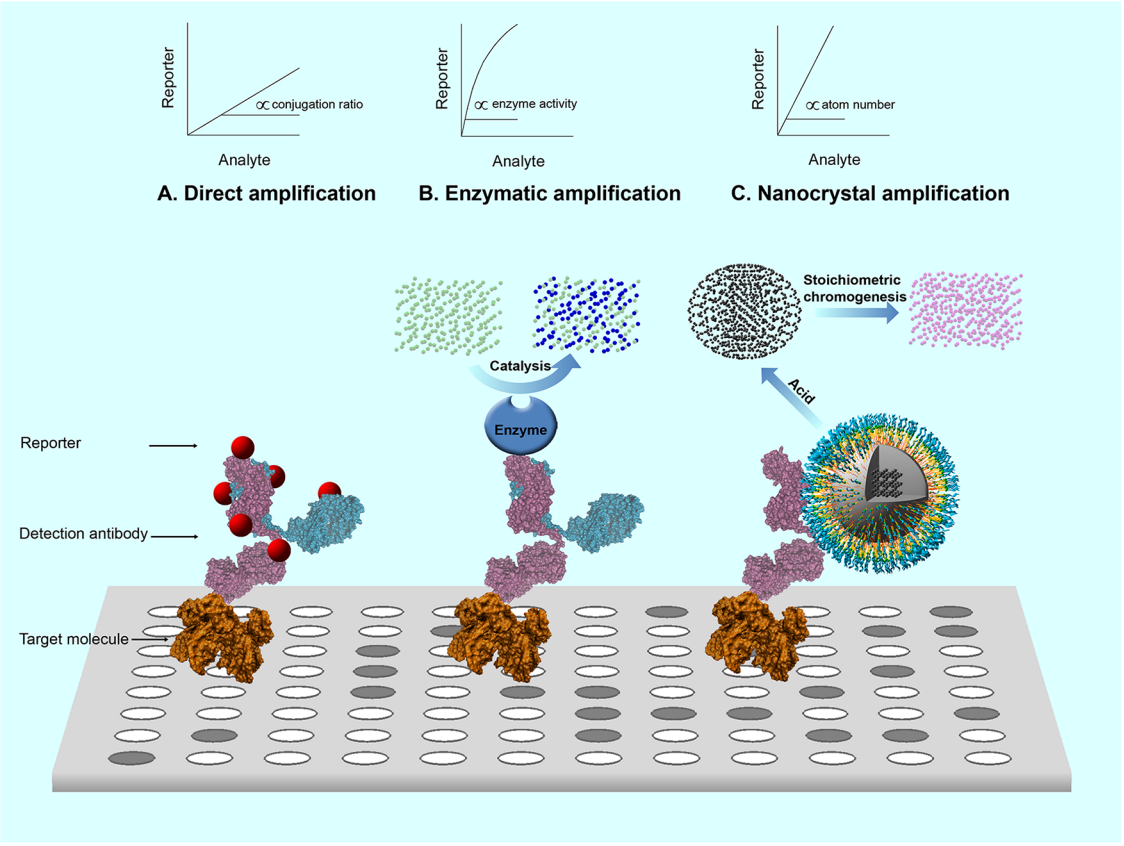

Scheme 1. Schematic representation of signal amplification schemes. In a typical detection assay, the target molecule is detected with probes, *e.g.*, antibodies or antibody fragments, that are linked to reporters *via* different amplification schemes. (A) Direct amplification. Reporters are conjugated or adsorbed to the probe surface. The amount of bound reporters is limited by the surface area and the number of docking sites on the probe. (B) Enzymatic amplification. The enzyme associated with the detection probe catalyzes hydrolysis of substrate molecules to generate an optical signal. The signal intensity is determined by the amount of hydrolyzed substrate, which is controlled by multiple factors such as enzyme activity, substrate concentration and incubation conditions. (C) Nanocrystal amplification. The nanocrystal conjugated with the probe is dissolved by acid into individual metal atoms which are converted to chromophores through a stoichiometric reaction. Signal amplification is fully determined by the total number of atoms in the nanocrystals bound to a single target molecule.

exceeds a few hundreds even with nano- or macroparticle based probes.[6] Consequently, the techniques employing direct amplification demand ultrasensitive reporters such as radioisotopes, which often rely on specialized instrument for signal acquisition.[6−14] In contrast, in enzymatic amplification, the detection probe is linked to an enzyme that can catalyze hydrolysis of chromogenic substrate (Scheme 1B). Enzyme-based amplification has been extensively used in immunosorbent assays and blotting assays for sensitive analyte detection. In particular, enzyme linked immunosorbent assay (ELISA) has been the industrial standard for quantification of protein and other macromolecule since its emergence in 1970s.[15,16] However, enzyme−substrate interaction is subjected to a number of variables such as enzymatic activity and incubation conditions. Biomolecule quantification with enzyme-linked probes is hindered by the requirement of stringent control, costly calibration as well as the nonlinear nature of enzymatic catalysis. Although ICP-MS linked assays have been used to measure ions in solution for immunoassays, in general they are time-consuming, costly, and yield low-throughput compared with ELISA.[13]

Here we present a novel signal amplification scheme exploiting the dense atom packing in metallic nanocrystals (Scheme 1C). In this assay format, after the antibody-functionalized nanocrystals bind to the target molecules (*e.g.,* antigen) and unbound ones removed, the nanocrystals are dissolved into individual metal ions that are then converted to chromophores. Signal amplification is fully determined by the total number of atoms in the nanocrystals bound to single target molecules. Although miniature in size, metallic nanocrystals consist of thousands to millions of metal atoms that can be readily extracted through acid dissolution (Table 1). Metal ion-induced chromogenesis has long been employed for photometric determination of trace metals.[17] Therefore, by dissolving nanocrystals to individual ions that are stoichiometrically converted to chromophores and quantified photometrically, extremely high signal amplification can be achieved.

The nanocrystal amplification scheme can be implemented with a rich selection of metal/metal oxide

TABLE 1. Wüstite Nanocrystals: Atom Counts and Detection Sensitivity

diameter (nm)	5	10	20	50	100
Number of iron atoms[a]	3,118	24,941	199,530	3,117,649	24,941,194
Detection limits[b]	32 fmol	4 fmol	501 amol	32 amol	4 amol

[a] The number of Fe atoms per nanocrystal was estimated with eq 2. [b] The detection limits of wüstite nanocrystals are calculated for ferrozine assay performed in 96-well plates with the detection limit of ferrous ions equal to 0.1 nmol (Figure 1A).

nanocrystals and metal-reactive chromogenic substrates. The chromogenic reactions can be either solution-based or surface-based and performed in aqueous or organic phase, supporting a variety of assay formats.[17] Here we demonstrate the amplification scheme by integrating the synthesis and functionalization of wüstite ($Fe_{1-x}O$) nanocrystals and robust ferrous ion-induced chromogenesis in immunosorbent assays and Western blot. Our studies show that the nanocrystal amplification is simple, highly sensitive and more reliable compared to enzymatic amplification. Owing to its superior stability and linearity, the nanocrystal amplification not only facilitates quantification of biomolecule concentration and binding kinetics in laboratory settings, but also empowers instrument-free evaluation of disease markers for on-site diagnostics. This amplification scheme can be applied to nearly all metal/metal oxide nanocrystals, greatly enriching the perspective of current nanoparticle-based bioassays.

RESULTS AND DISCUSSION

Wüstite Nanocrystal-Based Detection Scheme. Iron oxide nanoparticles (IONP) have received extensive research interests for applications in recording media, solid state batteries, chemical catalysts, detection assays, magnetic resonance imaging and drug/gene delivery.[9−11,18−20] We chose IONPs as the detection probes to take advantage of the well-developed synthesis method for convenient size control.[21−28] It is also noteworthy that Fe element only presents at low abundance in a few proteins such as ferritin, hemoglobin, transferrin and cytochromes, *etc.* in most biological specimens. Among all six known forms of iron oxides, wüstite has the highest density of Fe atoms. Additionally, wüstite nanocrystals are weakly paramagnetic at all sizes, while maghemite (γ-Fe_2O_3) and magnetite (Fe_3O_4) switch from superparamagnetic to ferromagnetic state at 15−20 nm.[26,29,30] Large wüstite nanocrystals are free of interparticle magnetic interactions, a prerequisite for stable dispersion, and thus used in IONP probes.

Fe atoms in IONPs can be extracted and converted to individual ferrous ions (Fe^{2+}) by sequential treatments with acids and reducing agents. Among more than a dozen of Fe^{2+}-based chromogenic reactions, Fe^{2+} can form optically stable and water-soluble chelates with ferrozine molecules, the solution of which changes from transparent to sharp purple in appearance

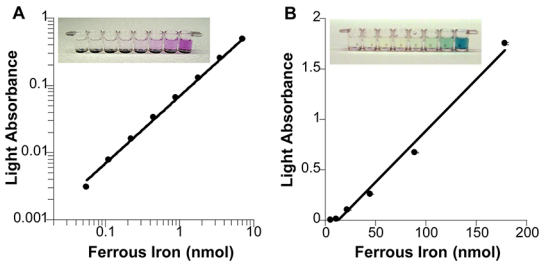

Figure 1. Fe ion-induced stoichiometric chromogenesis. (A) Ferrozine chelation. Fe^{2+} can be chelated by ferrozine, generating a sharp purple color. Light absorbance was measured at 562 nm with 810 nm as the reference. (B) Prussian blue reaction. Fe^{2+} can coordinate with potassium ferricyanide, the product of which is a bright blue colloid. Light absorption was measured at 790 nm immediately after reaction. All assays were performed in a 96-well microtiter plate (see insets). Mean of three measurements is plotted. Error bars showing standard deviations are plotted in B.

upon chelation ($\varepsilon_{562\ nm} = 2.79 \times 10^4\ M^{-1}\ cm^{-1}$) (Figure 1A).[17,31] In solution-based immunosorbent assays, IONPs can be measured by combining acid dissolution, reduction and ferrozine chelation. Fe^{2+} can also stoichiometrically react with potassium ferricyanide, resulting in either dispersed colloid or insoluble precipitates of Prussian blue (Figure 1B). The latter is useful for detecting IONPs in immunohistochemistry or blotting assays, which require semiquantification and localization of target molecules on a surface.

Using the nanocrystal amplification scheme, IONPs can achieve exceptional detection sensitivity. For example, there are 112,039 Fe atoms in a 16.5 nm wüstite nanocrystal. With the ferrozine method, the equivalent molar extinction coefficient of 16.5 nm wüstite nanocrystals, which is defined as the total light extinction of derived iron-ferrozine chelates, is $3.07 \times 10^9\ M^{-1}\ cm^{-1}$. To our knowledge, this is among the highest of all nanoparticles of similar size. Indeed, the equivalent molar extinction of wüstite nanocrystals is consistently higher than the molar extinction of gold nanospheres within the range of 1−100 nm (Figure 2). IONPs can be reliably measured at femtomole to attomole quantities in a 96-well microtiter plate, a standard format of immunosorbent assays (Table 1).

Iron Oxide Nanoparticle Synthesis and Functionalization. Wüstite nanocrystals with a uniform size distribution ($d = 16.5 \pm 1.9$ nm) were synthesized by solvent-free pyrolysis of iron acetylacetonate in oleic acid and oleylamine.[26] Larger nanocrystals can be obtained by changing the reaction conditions or the precursor compounds.[26,28] As-synthesized wüstite nanocrystals were dispersed in toluene. Water-dispersible IONPs were generated by coating the wüstite nanocrystals with a mixture of 1,2-distearoyl-*sn*-glycero-3-phosphoethanolamine-*N*-[methoxy(polyethylene glycol)-2000] (DSPE-mPEG) and 1,2-distearoyl-*sn*-glycero-3-phosphoethanolamine-*N*-[maleimide(polyethylene glycol)-2000] (DSPE-PEG-maleimide) using a dual solvent exchange

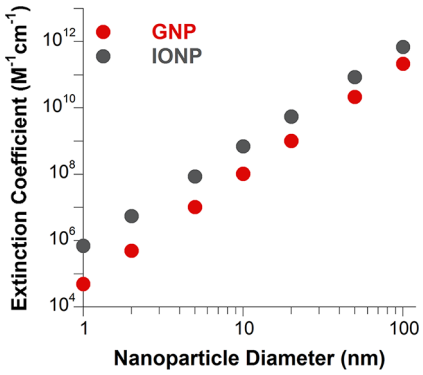

Figure 2. Extinction coefficients of wüstite nanocrystals and gold nanoparticles. The extinction coefficients of wüstite nanospheres are estimated based on ferrozine chelation. The extinction coefficients of gold nanospheres are calculated with a published equation.[39]

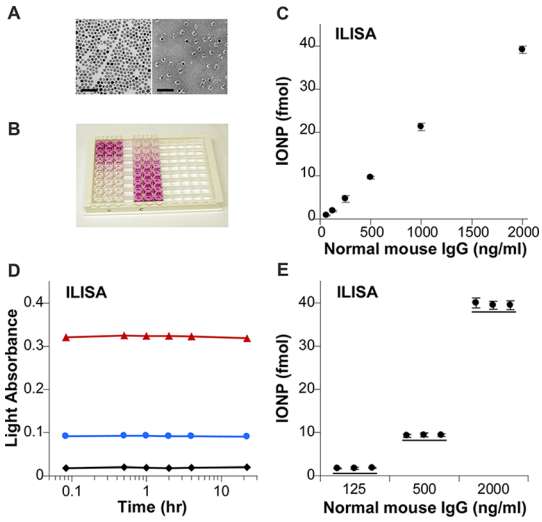

Figure 3. Applications of IONPs in direct immunosorbent assay. (A) TEM images of as-synthesized wüstite nanocrystals (16.5 nm) in toluene (left) and PEGylated and antibody-conjugated IONPs in water (right). The IONPs was negatively stained with methylamine tungstic acid. With negative staining, DSPE-PEG coating and antibody fragments on IONPs are visible as the white shell. Scale bar = 100 nm. (B) A representative image of color-developed ILISA strips. The left and the right three lanes are from the direct ILISA (C) and a competitive ILISA (Figure 4C), respectively. (C). In a direct ILISA, a 96-well microtiter plate was coated with normal mouse IgG at designated concentrations. Surface bound mouse IgG was detected with a goat antimouse IgG polyclonal antibody conjugated to 16.5 nm IONPs. (D) The temporal profile of light absorbance in the direct ILISA. From top to bottom were measured for 2000, 500, and 0 ng/mL mouse IgG. (E) Three independent measurements of mouse IgG with direct ILISA. Mean ± standard deviation of three measurements is plotted.

method.[32] The PEG layer reduces nonspecific binding of IONPs to the biomolecules, fulfilling a critical requirement of detection assays. Gel electrophoresis shows that the IONPs have uniform size distribution and maleimide density (Supporting Information Figure S1). The maleimide groups can be directly conjugated with thiolated antibody fragments, which can be obtained by antibody reduction with 2-mercaptoethylamine. For 16.5 nm wüstite nanocrystals, the resulting IONPs have an average hydrodynamic diameter of 39 nm as measured with dynamic light scattering. After the majority of empty DSPE-PEG micelles in the sample were removed using two rounds of ultracentrifugation, we performed negative staining of functionalized IONPs and a thin layer of DSPE-PEG together with conjugated antibodies is visible as the white shell in the TEM image (Figure 3A).

Nanocrystal Amplification in Solution-Based Detection: Immunosorbent Assays. To demonstrate the nanocrystal amplification scheme in solution-based detection, we developed the iron oxide nanoparticle linked immunosorbent assay (ILISA). Immunoglobulin G (IgG) is an important biomarker for many infectious diseases and autoimmune diseases, and has been used as a major detection probe in bioassays. There is a great need for determining IgG concentration and binding affinity in various specimens such as serum, ascites fluid and cell culture media. We selected mouse IgG as the target molecule (herein referred to as analyte) in ILISA and commercially available antibodies as the capture and detection antibodies. All reagent concentrations were chosen according to published ELISA protocols (Supporting Informaton Table 1).[33] IONP-based probes were prepared by conjugating wüstite nanocrystals (d = 16.5 ± 1.9 nm) with detection antibodies. The concentration of IONPs in the assay was determined in a kinetics study (Supporting Informaton Figure S2).

In a direct ILISA, the mouse IgG was detected with IONPs conjugated with a goat antibody. The IONPs bound to the surface-adsorbed analyte can be measured in a simple 20-min procedure (Figure 3B). In contrast to traditional ELISA (Supporting Informaton Figure S3), the direct ILISA attained perfect linearity over a wide range of concentrations (Figure 3C). In addition, the optical signals of ILISA remained constant for more than 24 h and the variations among independent experiments were less than 5%, demonstrating the exceptional repeatability of ILISA (Figure 3D,E). Thus, ILISA eliminates the need of calibration for each experiment, which significantly reduces the cost and the labor required by ELISA or radioimmunoassays (RIA).

Note that when the analyte concentration was 2000 ng/mL, the amount of bound IONPs was 39.1 fmol. Assuming all bound IONPs were located within the same plane near the bottom of the well (area = 0.32 cm^2), the interparticle distance was 41.6 nm, slightly larger than the hydrodynamic diameter of the IONPs. Further increasing the analyte concentration would cause deviation from linearity. Indeed, we found that the bound IONPs leveled off at 51.1 fmol with an analyte concentration of 4000 ng/mL (Supporting Informaton Figure S4). When larger IONPs were used, saturation was reached at a lower analyte concentration. Therefore, the top detection limit in ILISA is determined by steric hindrance to nanoparticle

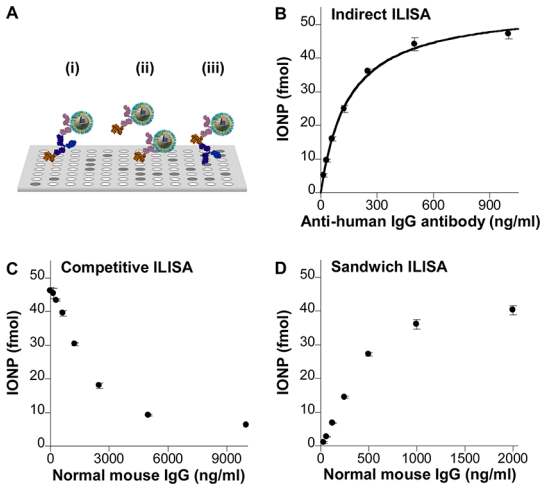

Figure 4. Application of IONPs in major forms of immunosorbent assays. (A) Schematic diagrams of indirect (i), competitive (ii), and sandwich (iii) ILISA. Shown in panels B, C, and D, respectively, are results of indirect, competitive, and sandwich ILISA assays performed with 16.5 nm IONPs conjugated with goat anti-mouse IgG antibody. The details of the experimental settings are included in Supporting Informaton Table S1. In panel B, the curve was fitted with eq 1. Mean ± standard deviation of three measurements is plotted.

binding: the distance between protein molecules at high coating density limits free access of IONPs.

Other IONP-based immunosorbent assays, including indirect, competitive and sandwich ILISA, had excellent performance as well (Figure 4). The indirect immunosorbent assay, in which the probe detects capture molecules binding to their target on the plate surface, is of great importance in screening unknown antibodies raised against a given antigen. In the indirect ILISA, the bound IONPs increased with the concentration of a mouse antibody targeting human IgG immobilized on the plate surface (Figure 3B). If the amount of bound IONPs were linearly proportional to the analyte concentration as determined in the direct ILISA, the results should reflect the binding kinetics between the mouse antibody and human IgG. Assuming that (1) each mouse antibody bound to only one epitope of human IgG and (2) the binding reached equilibrium, the quantity of bound IONPs, NP, should be governed by the following equation,

$$NP = \frac{NP_{max} \times C_A}{K_d + C_A} \quad (1)$$

where NP_{max} is the saturation level of NP, C_A is the concentration of the mouse antibody in solution and K_d is the dissociation constant between the mouse antibody and its antigen. As expected, the experimental results were fitted well by eq 1 with R^2 equal to 0.997 (Figure 4B). K_d of the mouse antibody binding to its antigen is estimated to be 147 ng/mL or 0.978 nM, in line with the antibody affinity reported in the literature.[34,35] This analysis reveals that in addition to antibody concentration, indirect ILISA can accurately delineate antibody−antigen interaction, providing a simple assay for antibody affinity.

The competitive immunosorbent assay quantifies proteins using one detection antibody and a plate coated with the purified analyte proteins. In the competitive ILISA, the plate precoated with mouse IgG was incubated with a mixed solution of the antibody-conjugated IONPs and free mouse IgG. The amount of bound IONPs decreased as the concentration of free mouse IgG increased over a large concentration range (Figure 4C). Since there were up to six antigen-binding sites on each IONP, it required a higher concentration of free analyte to fully inhibit the binding of the IONPs to surface-bound analyte, thus expanding the detection limit of the assay.

The sandwich immunosorbent assay, utilizing a pair of complementary antibodies for immobilization and detection of the analyte, is widely used for quantifying proteins in complex biological samples due to its excellent specificity and sensitivity. Similar to the indirect ILISA, the amount of bound IONPs in sandwich ILISA is governed by the binding kinetics between the capture antibody and the analyte (Figure 4D). A good linearity was attained for IgG concentrations between 31.3 to 500 ng/mL. Within this range, the sandwich ILISA was found three times more sensitive than the direct ILISA, presumably due to better antigen accessibility (Figures 3C and 4D).

Tunable Signal Amplification of IONP-Based Detection. Signal amplification of ILISA can be further optimized by varying the size and number of nanocrystals bound to an individual analyte molecule. By increasing the core size of IONPs from 16.5 to 28.8 nm ($d = 28.8 \pm 4.4$ nm), the signal intensity of a sandwich ILISA was increased by 5.89-fold, consistent with the volume ratio between the two nanocrystals (Figure 5B and Supporting Informaton Figure S5). As in traditional immunosorbent assays, the detection sensitivity of ILISA can be further enhanced by amplification with secondary IONPs. As illustrated in Figure 5A, the analyte was initially detected by goat antibody conjugated 16.5 nm IONPs, which were in turn bound by secondary probes of 28.8 nm IONPs conjugated with a rabbit anti-goat IgG antibody. With this two-step approach, the amplification was increased by 18.84-fold compared with using 16.5 nm probes alone and mouse IgG was detected at 0.59 ng/mL or 3.9 pM. Interestingly, the fold increase in amplification can be attributed to having one 16.5 nm probe bounded by three 28.8 nm probes per analyte ($1 + 3 \times 5.89 = 18.67$ *vs* 18.84). It is likely that the exact amount of signal enhancement depends on the sizes of the small and large nanoparticles, and the average number and accessibility of binding sites on the small nanoparticles.

IONP-Based Detection in Complex Biological Specimens. A potential issue is the interference between metal ions/chelators and iron-ferrozine chelation, especially

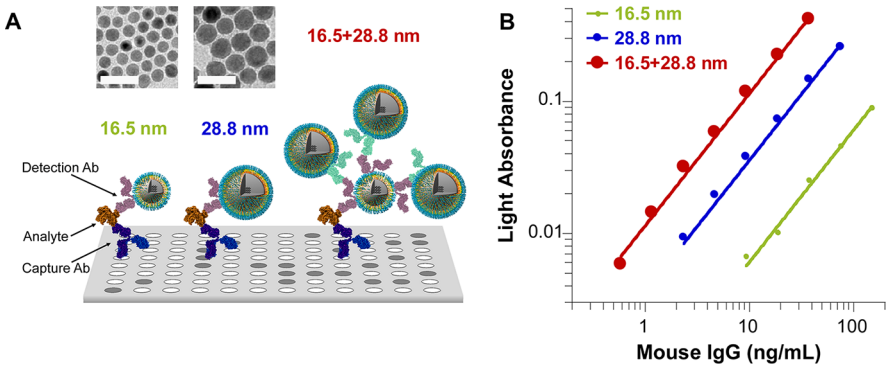

Figure 5. Signal amplification in ILISA. (A) Schematic diagrams of signal amplification employed in panel B for enhanced detection sensitivity in sandwich ILISA. In the control study, mouse IgG was detected with the 16.5 nm IONPs linked to goat antibody. To improve the detection sensitivity, one can either replace the 16.5 nm IONPs with larger IONPs (28.8 nm) or detect the antibody fragments on the 16.5 nm IONPs using secondary IONPs (28.8 nm IONPs conjugated with a rabbit antibody raised against goat IgG). Mean of three measurements and fitted lines are plotted. The same data plotted with error bars in linear scale is provided in Supporting Informaton Figure S5. Insets in panel A are TEM images of 16.5 and 28.8 nm wüstite nanocrystals, respectively. Scale bar = 50 nm.

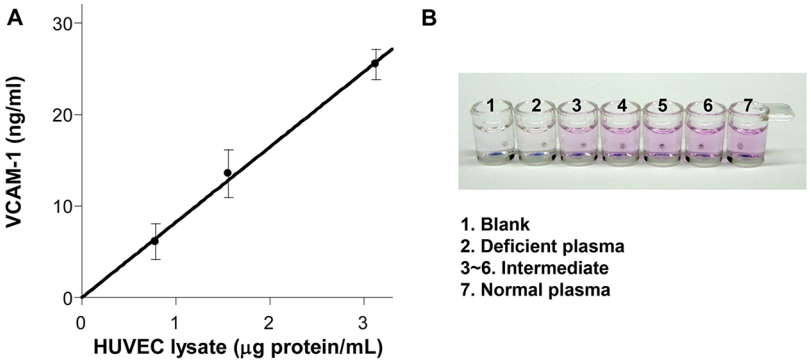

Figure 6. Specific applications of ILISA. (A) VCAM-1 in the lysate of LPS-stimulated HUVEC was quantified with a sandwich ILISA. Mean ± standard deviation of three measurements is plotted. (B) Instrument-free distinction of factor-X deficient *vs* normal human plasma. Factor X in human plasma was detected with a sandwich ILISA.

when biological specimens are used. However, we found that sandwich ILISA could be performed with cell homogenate and plasma, the two most common types of biological samples, without special handling. This indicates that routine capture and wash steps in a bioassay can effectively eliminate interfering compounds. Specifically, human umbilical vascular endothelial cells (HUVEC) were cultured with M199 medium containing Ca^{2+}, Fe^{3+} and Mg^{2+}. Vascular cell adhesion molecule-1 (VCAM-1), an inflammatory marker, could be detected by sandwich ILISA in the lysate of lipopolysaccharide (LPS)-stimulated HUVECs at low total protein concentration (1 μg/mL) while achieving a good linearity (Figure 6A and Supporting Informaton Figure S6).

Sandwich ILISA could also detect factor-X, a blood coagulation factor that is screened clinically for inherited or acquired factor X deficiency, in clinical plasma samples (Supporting Informaton Figure S7). Importantly, with optimized sample dilution, the difference between a factor X-deficient patient and a healthy individual could be distinguished with the naked eye (Figure 6B).

Nanocrystal Amplification in Surface-Based Detection: Western Blot. In blotting assays, biomolecules such as proteins and nucleic acids distributed on a membrane needs to be localized and detected quantitatively. As mentioned above, Prussian blue staining allows *in situ* detection of IONPs bound on a surface. As an example, a Western blot was performed for mouse IgG at designated quantities. Bovine serum albumin (BSA) was used as the negative control. After the proteins were transferred onto a cellulose membrane, mouse IgG was detected with 16.5 nm IONPs conjugated with a rabbit anti-mouse IgG antibody (Figure 7A). The protein bands were visualized by simply incubating the membrane in a solution containing HCl and potassium ferrocyanide. All fragments of mouse IgG can be observed because of the polyclonal nature of the detection antibody. The intensity of the bands correlated well with the quantities of mouse IgG. Mouse IgG was detected at an amount of 31 ng or 0.21 pmol, while BSA was visible with the nonspecific Coomassie blue staining but not with the IONPs (Figures 7). Similar to ILISA, the detection sensitivity of IONPs can be further improved by using large

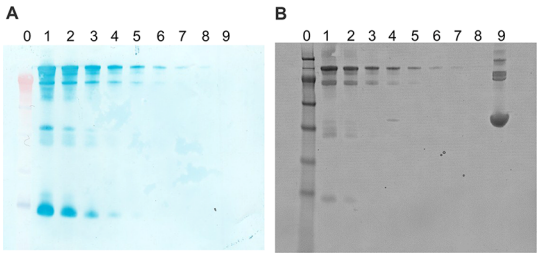

Figure 7. Application of IONPs in Western blot. Mouse IgG and BSA were analyzed with gel electrophoresis in Nuge 4–12% Bis-Tris gel. (A) Protein bands transferred to a cellulose membrane were detected with 16.5 nm IONPs conjugated with rabbit anti-mouse IgG polyclonal antibody. (B) In a parallel preparation, protein bands in polyacrylamide gel were stained with Coomassie blue. In A and B, molecular weight markers and BSA were loaded to lane 0 and lane 9, respectively. From lane 1 to lane 8, the amounts of mouse IgG are 4000, 2000, 1000, 500, 250, 125, 62.5, and 31.25 ng.

nanoparticles or combinations of nanoparticles. Therefore, IONPs are capable of highly specific, sensitive and semiquantitative detection on cellulose membranes.

CONCLUSIONS

Over the past decade, the need for simple, sensitive and reliable biomolecule quantification techniques has stimulated an extensive search for improved detection schemes. Among these approaches, gold nanoparticles and quantum dots often become the probe of choice, largely because of their stable optical properties derived from quantum confinement of electrons or excitons in the nanocrystal.[3,4,36] In contrast, the signal amplification scheme presented here is based on the number of metal atoms in a nanocrystal, which is very robust and largely determined by its size distribution once the type of nanocrystal is chosen. This novel signal amplification scheme can be applied to most metal/metal oxide nanocrystals using acid dissolution and metal-induced chromogenesis, greatly expanding the arsenal of nanoparticle-based detection methods. The numerous combinations of metal-induced chromogenesis and nanocrystals of various sizes and compositions can lead to a wide range of potential biomedical applications. In particular, since nearly all metal ions can generate chromophores in a stoichiometric manner, it is possible to have multiplexed biomolecule detection by combining orthogonal chromogenesis of different metallic nanocrystals in the same assay. For example, Co^{2+}, Cu^{2+} and Fe^{2+} can be measured simultaneously with ferrozine alone using the distinct absorption peaks of corresponding metal chelates.[37]

Two distinctive advantages of the nanocrystal-enabled amplification scheme are exceptional repeatability and instrument-free detection. In many laboratory and clinical applications, samples need to be examined one at a time. In contrast to RIA or ELISA, ILISA eliminates the need of repetitive calibration for each individual experiment. Once commercialized, each batch of ILISA reagent may only need to be calibrated once before packaging and distribution. Therefore, with ILISA, a single measurement can be performed and the biomolecule concentration be calculated with the precalibrated curve ("standard curve") included in the data sheet of the reagent, which significantly reduces the cost and the labor required by traditional assays. Further, thanks to the repeatability and tunable dynamic range of ILISA, it allows "instrument-free" detection of many disease markers that vary significantly between healthy and disease states. The IONP-based "instrument-free" detection kits can be a valuable diagnostic tool for on-site medical service or patient screening in developing countries where advanced instruments are not available.

The nanocrystal-based amplification scheme features a very large amplification factor that can be tuned through nanocrystal size and sequential detection, while keeping the linearity preserved. Even without optimization, the detection limit of ILISA reaches low-picomolar level, covering a wide dynamic range of disease markers. The detection sensitivity can be further improved by using large nanocrystals (>30 nm) or even microparticles consisting of clusters of nanocrystals. An alternative approach is to take advantage of fluorogenesis reactions. For example, the detection limit of magnesium with bis-salicylidene-ethylenediamine is 3 orders of magnitude higher than iron-ferrozine chelates, having the potential for ultrasensitive detection.[38] It is also conceivable to incorporate the nanocrystal-based quantification scheme in other bioassay formats such as those using microfluidics and microarrays.

METHODS

Materials. Iron(III) acetylacetonate (99.9%), oleic acid (90%), oleylamine (70%), toluene (99.9%), chloroform (99%), DMSO (99.9%), hydrochloric acid, hydroxylamine HCl, sodium hydroxide, ammonium acetate, ferrozine, potassium ferrocyanide, iodoacetamide and lipopolysaccharide (LPS) were purchased from Sigma-Aldrich. 1,2-Distearoyl-*sn*-glycero-3-phosphoethanolamine-*N*-[methoxy(polyethylene glycol)-2000] (DSPE-mPEG) and 1,2-distearoyl-*sn*-glycero-3-phosphoethanolamine-*N*-[maleimide(polyethylene glycol)-2000] (DSPE-PEG-maleimide) were purchased from Avanti Polar Lipids. 2-Mercaptoethylamine-HCl (MEA) was purchased from Thermo Scientific. All chemicals were used without modification.

Normal mouse IgG and ABTS kit were purchased from Vector Laboratories. Normal human IgG, goat anti-mouse IgG polyclonal antibody and rabbit anti-goat IgG polyclonal antibody, mouse anti-human VCAM-1 monoclonal antibody, goat anti-human VCAM-1 polyclonal antibody and recombinant human VCAM-1 were purchased from R&D systems. Rabbit anti-mouse IgG polyclonal antibody, mouse anti-human IgG monoclonal antibody, rabbit anti-human factor X polyclonal antibody and human factor X were purchased from Abcam. Horseradish peroxidase conjugated goat anti-mouse IgG polyclonal antibody was purchased from Santa Cruz Biotechnology. Human

factor X deficient plasma was purchased from Haematologic Technologies. HUVEC was purchased from Life Technologies and cultured according to vendor's instructions.

The 96-well ELISA plates were purchased from R&D systems. Vivaspin 20 centrifugal filter tubes (MW = 100K) were purchased from VWR International. Amicon centrifugal filter tubes (MW = 10K) were purchased from EMD Millipore.

Estimation of the Number of Fe Atoms per Wüstite Nanocrystal. Assuming a uniform fcc structure, a consistent molecular formula of FeO and a perfect spherical shape of wüstitite nanocrystals, the number of Fe atoms in each nanocrystal can be calculated with the following equation.

$$N = \rho N_A \frac{\pi D^3}{6M} \quad (2)$$

Where ρ is the density of bulk wüstite (5.7 g/cm^3), N_A is the Avogadro constant, D is the diameter of nanocrystals, and M is the molecular weight of wüstite (72 Da). Wüstite has a nonstoichiometric formula of $Fe_{1-x}O$ ($1 - x = 0.83-0.96$). But assuming a formula of FeO only leads to less than 5% overestimation of the atom number. The surface of wüstite nanocrystals can be slowly oxidized to other iron oxide upon long exposure to air. But this will not change the Fe atom number per nanocrystal. The average diameter of the wüstite nanocrystals used in this study was measured from TEM images of freshly synthesized nanocrystals with an automated program in ImagePro Plus software. At least 500 particles were counted for each type of nanocrystals.

Synthesis of Wüstite Nanocrystals. The 16.5 nm wüstite nanocrystals were synthesized using a modified protocol according to a previous publication.[26] Larger nanocrystals can be obtained using similar procedures.[26,28] First, 12 mmol $Fe(acac)_3$, 75 mmol oleic acid and 105 mmol oleylamine were added to a 250 mL three-neck round-bottom flask. The solution was mixed vigorously with a magnetic stir bar throughout the reaction. The reaction included three steps. First, the solution was incubated at 120 °C under partial vacuum for 2 h. After that, the flask was heated to 220 °C with a ramp rate of 5 °C/min and incubated at this temperature for 30 min under a flow of argon. Finally, the solution was heated to 300 °C with a ramp rate of 2 °C/min and incubated at this temperature for 30 min under argon. After the reaction, the heating mantle was removed and the solution was cooled to room temperature.

To collect synthesized wüstite nanocrystals, 100 mL absolute ethanol was added to the solution. The solution was centrifuged at 5000*g* at room temperature for 10 min and the supernatant was discarded. The black pellets could be easily dispersed with toluene. To remove free oleic acid and oleylamine in the solution, the nanocrystals were washed by ethanol precipitation two more times. After the last wash, the pellets were dried with a beam of argon gas and dispersed with toluene. To remove smaller nanocrystals, the toluene solution was mixed with ethanol at a ratio of 2:1 (v/v). The solution was centrifuged at 5000*g* at room temperature for 10 min and the pellets were collected. During this procedure, large nanocrystals precipitated preferentially due to higher surface energy.

Surface Coating and Maleimide Activation of Wüstite Nanocrystals. Water-dispersible and maleimide-functionalized iron oxide nanoparticles were synthesized by coating wüstite nanocrystals with amphiphilic DSPE-PEG copolymers using a dual solvent exchange method.[32] In a typical coating procedure, 0.4 mL of the nanocrystals (5 mg Fe/mL in toluene), 0.6 mL of DSPE-mPEG (10 mg/mL in chloroform), 0.09 mL of DSPE-PEG-maleimide (2 mg/mL in chloroform) and 1 mL of chloroform were mixed in a 250 mL flask. Eight milliliters of DMSO was added to the flask dropwise with gentle shaking over a period of 20 min. Then the flask was connected to a vacuum pump to remove toluene and chloroform from the mixture. The evaporation was stopped when the solution weighed 7.04 g. After that, 30 mL of distilled water was slowly added to the DMSO solution and DMSO was removed by solvent exchange with Vivaspin centrifugal filter tubes (MW = 100K). To remove empty micelles formed by DSPE-mPEG and DSPE-PEG-maleimide, the solution was centrifuged twice (50 000*g*, 4 °C and 1 h). At the end of centrifugation, the pellet was dispersed with distilled water. For 16.5 nm wüstite nanocrystals, the resulting IONPs had an average hydrodynamic diameter of 39 nm as measured with dynamic light scattering (DynaPro Nanostar, Wyatt Technology). Gel electrophoresis shows that the IONPs had a highly uniform size distribution and maleimide density (Supporting Information Figure S1). In addition, maleimide is available for antibody conjugation for at least 24 h if IONPs are dispersed in distilled water at 4 °C.

Conjugation of Antibodies to IONPs. The antibodies were reduced with 2-mercaptoethylamine-HCl (MEA). Reduced antibody fragments with free sulfhydryl groups were conjugated to maleimide activated IONPs through thiol-maleimide reaction. In a typical reaction, 100 μg antibody was mixed with MEA in 200 μL PBS-EDTA (100 mM phosphate, 10 mM EDTA and pH 7.2) and incubated at 37 °C for 2 h. The concentrations of MEA were 30 mM for rabbit antibodies and 100 mM for goat and sheep antibodies. Reduced antibody fragments were washed five times with sodium acetate (100 mM, pH 5.5) in Amicon centrifugal filter tubes (MW = 10K). After washes, IgG concentration was determined by light absorption at 280 nm ($A_{280\ nm} = 1.36$ for 1 mg/mL IgG). The IONPs were mixed with reduced IgG at 1:3 molar ratio (*e.g.*, 72 μg antibody fragments for each 1000 μg Fe of 16.5 nm IONPs) in PBS. The antibody concentration in the reaction mixture was fixed at 100 nM. The solution was incubated at room temperature overnight. After conjugation, the solution was centrifuged twice (50 000*g*, 4 °C and 1 h) and supernatant with unconjugated antibody fragments was discarded.

Protein Coating of 96-Well Microtiter Plates. In ILISA or ELISA, the plates were prepared in two steps. First, purified capture antibodies or antigens were adsorbed to the plate surface. Then, the plate surface was saturated with BSA to prevent nonspecific interactions between the plate surface and other protein molecules. For example, to prepare the plate for the direct immunosorbent assay, 100 μL of normal mouse IgG at designated concentrations was added to each well. The plate was covered with a sealer and incubated at 4 °C for 24 h. After incubation, the plate was washed three times with PBS containing 0.05% Tween-20. Each well was filled with 300 μL of 1% BSA in PBS. After incubated at 4 °C for another 24 h, the plate was ready to use. The plates used in other ILISAs were prepared similarly (Supporting Information Table S1).

Detecting Surface-Bound Proteins with IONPs in 96-Well Plates. Antigen bound 96-well plates were prepared according to the standard ELISA protocol (Supporting Information Table S1). In a typical ILISA, 16.5 nm IONP-based probes were diluted with PBS containing 1% BSA to a final concentration of 100 μg Fe/mL. A total of 100 μL of IONP solution was added to each well. The plate was cover with a plate sealer and incubated at 37 °C for 1 h with vigorous shaking. After incubation, the plate was decanted and washed with PBS containing 0.05% Tween-20. To measure Fe atoms of bound IONPs, the wells were incubated with 50 μL of 6 M HCl at room temperature for 15 min. Then, 70 μL of 4 M NaOH and 80 μL of color development solution were sequentially added to each well. The color development solution was made by mixing 1.5 mL 7.5 M ammonium acetate, 2.5 mL 5% hydroxylamine hydrochloride solution and 4 mL 0.1% ferrozine solution immediately before use. After mixing with pipettes, the light absorbance of the solutions was measured at 562 nm with 810 nm as the reference using a microplate reader.

Application of IONPs in Western Blot. Mouse IgG at designated quantities and BSA were analyzed with gel electrophoresis in Nuge 4–12% Bis-Tris gel. After the protein bands were transferred onto a cellulose membrane, mouse IgG was detected with 16.5 nm IONPs conjugated with a rabbit anti-mouse IgG polyclonal antibody. In brief, the membrane was blocked with non-fat milk at room temperature for 60 min. Then, the membrane was incubated with the IONP solution (100 μg/mL in PBS with 1% BSA) at room temperature for 60 min. After washes, the membrane was immersed in a solution containing 2% potassium ferrocyanide and 2 M HCl, and sharp blue bands appeared after 5 min incubation. The membrane was imaged with an office scanner.

Conflict of Interest: The authors declare no competing financial interest.

Acknowledgment. This work was supported by the National Heart Lung and Blood Institute of the NIH as a Program of Excellence in Nanotechnology award (HHSN268201000043C to G.B.).

Supporting Information Available: Table listing the reagent concentrations in ELISA and ILISA experiments; distribution and stability of maleimide groups on IONPs; binding avidity of antibody-conjugated IONPs; direct ELISA; steric hindrance in immunosorbent assays; signal amplification in sandwich ILISA; quantification of cellular VCAM-1 and human factor X. This material is available free of charge *via* the Internet at http://pubs.acs.org.

REFERENCES AND NOTES

1. Zangar, R. C.; Daly, D. S.; White, A. M. ELISA Microarray Technology as a High-Throughput System for Cancer Biomarker Validation. *Expert Rev. Proteomics* **2006**, *3*, 37–44.
2. Schupbach, J. Measurement of HIV-1 P24 Antigen by Signal-Amplification-Boosted ELISA of Heat-Denatured Plasma is a Simple and Inexpensive Alternative To Tests for Viral RNA. *AIDS Rev.* **2002**, *4*, 83–92.
3. Peng, H. I.; Miller, B. L. Recent Advancements in Optical DNA Biosensors: Exploiting the Plasmonic Effects of Metal Nanoparticles. *Analyst* **2011**, *136*, 436–447.
4. Alivisatos, P. The Use of Nanocrystals in Biological Detection. *Nat. Biotechnol.* **2004**, *22*, 47–52.
5. Dykman, L.; Khlebtsov, N. Gold Nanoparticles in Biomedical Applications: Recent Advances and Perspectives. *Chem. Soc. Rev.* **2012**, *41*, 2256–2282.
6. Nam, J. M.; Thaxton, C. S.; Mirkin, C. A. Nanoparticle-Based Bio-Bar Codes for the Ultrasensitive Detection of Proteins. *Science* **2003**, *301*, 1884–1886.
7. Nam, J. M.; Stoeva, S. I.; Mirkin, C. A. Bio-Bar-Code-Based DNA Detection with PCR-Like Sensitivity. *J. Am. Chem. Soc.* **2004**, *126*, 5932–5933.
8. Chin, C. D.; Laksanasopin, T.; Cheung, Y. K.; Steinmiller, D.; Linder, V.; Parsa, H.; Wang, J.; Moore, H.; Rouse, R.; Umviligihozo, G.; *et al.* Microfluidics-Based Diagnostics of Infectious Diseases in the Developing World. *Nat. Med.* **2011**, *17*, 1015–1019.
9. Perez, J. M.; Josephson, L.; O'Loughlin, T.; Hogemann, D.; Weissleder, R. Magnetic Relaxation Switches Capable of Sensing Molecular Interactions. *Nat. Biotechnol.* **2002**, *20*, 816–820.
10. Lin, P. C.; Chou, P. H.; Chen, S. H.; Liao, H. K.; Wang, K. Y.; Chen, Y. J.; Lin, C. C. Ethylene Glycol-Protected Magnetic Nanoparticles for a Multiplexed Immunoassay in Human Plasma. *Small* **2006**, *2*, 485–489.
11. Burtea, C.; Laurent, S.; Roch, A.; Vander Elst, L.; Muller, R. N. C-MALISA (Cellular Magnetic-Linked Immunosorbent Assay), a New Application of Cellular ELISA for MRI. *J. Inorg. Biochem.* **2005**, *99*, 1135–1144.
12. Yalow, R. S.; Berson, S. A. Immunoassay of Endogenous Plasma Insulin in Man. *J. Clin. Invest.* **1960**, *39*, 1157–1175.
13. Quinn, Z. A.; Baranov, V. I.; Tanner, S. D.; Wrana, J. L. Simultaneous Determination of Proteins Using an Element-Tagged Immunoassay Coupled with ICP-MS Detection. *J. Anal. At. Spectrom.* **2002**, *17*, 892–896.
14. Merkoci, A.; Aldavert, M.; Tarrason, G.; Eritja, R.; Alegret, S. Toward an ICPMS-Linked DNA Assay Based on Gold Nanoparticles Immunoconnected through Peptide Sequences. *Anal. Chem.* **2005**, *77*, 6500–6503.
15. Engvall, E.; Perlmann, P. Enzyme-Linked Immunosorbent Assay (ELISA) Quantitative Assay of Immunoglobulin-G. *Immunochemistry* **1971**, *8*, 871–874.
16. Vanweeme, Bk; Schuurs, A. H. W. Immunoassay Using Antigen-Enzyme Conjugates. *FEBS Lett.* **1971**, *15*, 232–236.
17. Sandell, E. B.; Onishi, H. *Photometric Determination of Traces of Metals*, 4th ed.; Wiley: New York, 1978.
18. Gao, L.; Zhuang, J.; Nie, L.; Zhang, J.; Zhang, Y.; Gu, N.; Wang, T.; Feng, J.; Yang, D.; Perrett, S.; *et al.* Intrinsic Peroxidase-Like Activity of Ferromagnetic Nanoparticles. *Nat. Nanotechnol.* **2007**, *2*, 577–583.
19. Poizot, P.; Laruelle, S.; Grugeon, S.; Dupont, L.; Tarascon, J. M. Nano-Sized Transition-Metal Oxides as Negative-Electrode Materials for Lithium-Ion Batteries. *Nature* **2000**, *407*, 496–499.
20. Xie, J.; Liu, G.; Eden, H. S.; Ai, H.; Chen, X. Surface-Engineered Magnetic Nanoparticle Platforms for Cancer Imaging and Therapy. *Acc. Chem. Res.* **2011**, *44*, 883–892.
21. Kolesnichenko, V. L.; Caruntu, D.; Caruntu, G.; Chen, Y.; O'Connor, C. J.; Goloverda, G. Synthesis of Variable-Sized Nanocrystals of Fe_3O_4 with High Surface Reactivity. *Chem. Mater.* **2004**, *16*, 5527–5534.
22. Weissleder, R.; Elizondo, G.; Wittenberg, J.; Rabito, C. A.; Bengele, H. H.; Josephson, L. Ultrasmall Superparamagnetic Iron Oxide: Characterization of a New Class of Contrast Agents for MR Imaging. *Radiology* **1990**, *175*, 489–493.
23. Sun, S.; Zeng, H.; Robinson, D. B.; Raoux, S.; Rice, P. M.; Wang, S. X.; Li, G. Monodisperse MFe_2O_4 (M = Fe, Co, Mn) Nanoparticles. *J. Am. Chem. Soc.* **2004**, *126*, 273–279.
24. Jana, N. R.; Chen, Y. F.; Peng, X. G. Size- and Shape-Controlled Magnetic (Cr, Mn, Fe, Co, Ni) Oxide Nanocrystals *via* a Simple and General Approach. *Chem. Mater.* **2004**, *16*, 3931–3935.
25. Jun, Y. W.; Huh, Y. M.; Choi, J. S.; Lee, J. H.; Song, H. T.; Kim, S.; Yoon, S.; Kim, K. S.; Shin, J. S.; Suh, J. S.; *et al.* Nanoscale Size Effect of Magnetic Nanocrystals and Their Utilization for Cancer Diagnosis *via* Magnetic Resonance Imaging. *J. Am. Chem. Soc.* **2005**, *127*, 5732–5733.
26. Hou, Y. L.; Xu, Z. C.; Sun, S. H. Controlled Synthesis and Chemical Conversions of FeO Nanoparticles. *Angew. Chem., Int. Ed.* **2007**, *46*, 6329–6332.
27. Hyeon, T.; Park, J.; An, K. J.; Hwang, Y. S.; Park, J. G.; Noh, H. J.; Kim, J. Y.; Park, J. H.; Hwang, N. M. Ultra-Large-Scale Syntheses of Monodisperse Nanocrystals. *Nat. Mater.* **2004**, *3*, 891–895.
28. Bronstein, L. M.; Atkinson, J. E.; Malyutin, A. G.; Kidwai, F.; Stein, B. D.; Morgan, D. G.; Perry, J. M.; Karty, J. A. Nanoparticles by Decomposition of Long Chain Iron Carboxylates: From Spheres to Stars and Cubes. *Langmuir* **2011**, *27*, 3044–3050.
29. Krishnan, K. M.; Pakhomov, A. B.; Bao, Y.; Blomqvist, P.; Chun, Y.; Gonzales, M.; Griffin, K.; Ji, X.; Roberts, B. K. Nanomagnetism and Spin Electronics: Materials, Microstructure and Novel Properties. *J. Mater. Sci.* **2006**, *41*, 793–815.
30. Sun, X.; Huls, N. F.; Sigdel, A.; Sun, S. Tuning Exchange Bias in Core/Shell FeO/Fe_3O_4 Nanoparticles. *Nano Lett.* **2012**, *12*, 246–251.
31. Stookey, L. L. Ferrozine—A New Spectrophotometric Reagent for Iron. *Anal. Chem.* **1970**, *42*, 779–781.
32. Tong, S.; Hou, S.; Ren, B.; Zheng, Z.; Bao, G. Self-Assembly of Phospholipid-PEG Coating on Nanoparticles through Dual Solvent Exchange. *Nano Lett.* **2011**, *11*, 3720–3726.
33. Ausubel, F. M. *Short Protocols in Molecular Biology: A Compendium of Methods from Current Protocols in Molecular Biology*, 5th ed.; Wiley: New York, 2002.
34. Friguet, B.; Chaffotte, A. F.; Djavadiohaniance, L.; Goldberg, M. E. Measurements of the True Affinity Constant in Solution of Antigen-Antibody Complexes by Enzyme-Linked Immunosorbent-Assay. *J. Immunol. Methods* **1985**, *77*, 305–319.
35. Nieba, L.; Krebber, A.; Pluckthun, A. Competition BIAcore for Measuring True Affinities: Large Differences from Values Determined from Binding Kinetics. *Anal. Biochem.* **1996**, *234*, 155–165.
36. Jans, H.; Huo, Q. Gold Nanoparticle-Enabled Biological and Chemical Detection and Analysis. *Chem. Soc. Rev.* **2012**, *41*, 2849–2866.
37. Kundra, S. K.; Katyal, M.; Singh, R. P. Spectrophotometric Determination of Copper(I) and Cobalt(II) with Ferrozine. *Anal. Chem.* **1974**, *46*, 1605–1606.
38. White, C. E.; Cuttitta, F. Fluorometric Study of the Magnesium-Bissalicylidene-Ethylenediamine System. *Anal. Chem.* **1959**, *31*, 2083–2087.
39. Liu, X.; Atwater, M.; Wang, J.; Huo, Q. Extinction Coefficient of Gold Nanoparticles with Different Sizes and Different Capping Ligands. *Colloids Surf., B* **2007**, *58*, 3–7.